

# Novel Fluidic Packaging of Gimbal-less MEMS Mirrors for Increased Optical Resolution and Overall Performance

Veljko Milanovic\*, Abhishek Kasturi, James Yang

Mirrorcle Technologies, Inc., 4905 Central Ave, Richmond, CA 94804

## 1. ABSTRACT

Gimbal-less two-axis quasistatic MEMS mirrors have the ability to reflect optical beams to arbitrary positions and with arbitrary velocity. This technology has become established in many applications including laser based tracking, 3D scanning, biomedical imaging, free-space communication, and LiDAR. However, for certain defense applications, the total angle  $\times$  diameter product, or the mirror's effective achievable resolution ( $\theta \times D$  product), has not been large enough to address requirements for agile steering in large fields of regard and with a low diffraction-limited beam divergence. Two key limitations have been the relatively low forces available in electrostatic combdrive actuators and the susceptibility of large-diameter MEMS mirrors to shock and vibrations.

In this work, we demonstrate that these same MEMS mirrors can have dramatically increased performance when fully immersed and packaged in dielectric liquids with highly favorable torque-increasing, damping-increasing, and optical gain-increasing properties. The rotating electrostatic combdrive has its torque multiplied by liquid's relative permittivity of  $\sim 2.5$ . Furthermore, by selecting the appropriate fluid viscosity, quality factor of the device is reduced and structural damping is tuned to near critical damping. Finally, the increased scan angle due to the  $\sim 1.5$ - $1.7$  index of refraction of the fluid is an additional benefit. These numerous benefits of the fluidic packaging enabled us to double and in some cases triple the previously achieved  $\theta \times D$  product of two-axis quasistatic MEMS mirrors while still maintaining speeds applicable for above mentioned applications. One of the most exciting benefits of the packaging methodologies is that the damping dramatically increases shock and vibration tolerance, which will be tested next.

Keywords: MEMS Mirrors, dielectric fluids, dielectric liquid, oil capacitor, electrostatic combdrive, MEMS damping, squeeze film damping.

## 2. INTRODUCTION

### 2.1 Gimbal-less two-axis quasistatic MEMS mirrors

Most of our gimbal-less MEMS mirror device types are designed and optimized for point-to-point optical beam steering. A steady-state analog actuation voltage results in a steady-state analog angle of rotation of the micromirror. Near DC, there is a one-to-one correspondence of actuation voltages and resulting angles: it is highly repeatable with no measurable degradation over time. A sequence of actuation voltages results in a sequence of mirror angles for point-to-point beam-steering. These devices can be operated over a very wide bandwidth from DC (maintaining position at constant voltage with nearly zero power consumption at the device) to several thousand Hertz with mechanical tilt range of  $-5^\circ$  to  $+5^\circ$  on each axis or larger depending on the design [1]. At higher frequencies closer to device resonance, the full device response must be taken into account; however, it can be generally stated that this technology enables arbitrary control of laser beam position and velocity up to a certain velocity limit. Such fast and broadband capability allows nearly arbitrary waveforms such as vector graphics, constant velocity line scanning, point-to-point step scanning, and resonant-quasistatic rastering (one axis resonant, the other quasi-static). These capabilities are utilized in established applications such as 3D scanning [2], biomedical imaging [3], free-space communication, LiDAR [4],[5], and laser tracking (Figure 1c) [6],[7].

The MEMS devices' actuators lend themselves inherently to a modular design approach. Each actuator can utilize electrostatic rotators (Figure 1a) of chosen length (depending on the allotted chip size), arbitrarily stiff linkages, and arbitrarily positioned mechanical rotation transformers [17]. In addition, the device can have an arbitrarily large mirror diameter [1],[20] – however naturally not without significant trade-offs. Devices with larger-diameter mirrors are correspondingly quadratically slower due to the increased inertia. Namely, inertia of a round mirror plate is proportional to the fourth power of its radius and therefore its speed is inverse proportional to the square of the radius. This is a general rule of thumb when comparing device designs, but many other parameters affect the actual performance especially die size and angle swing.

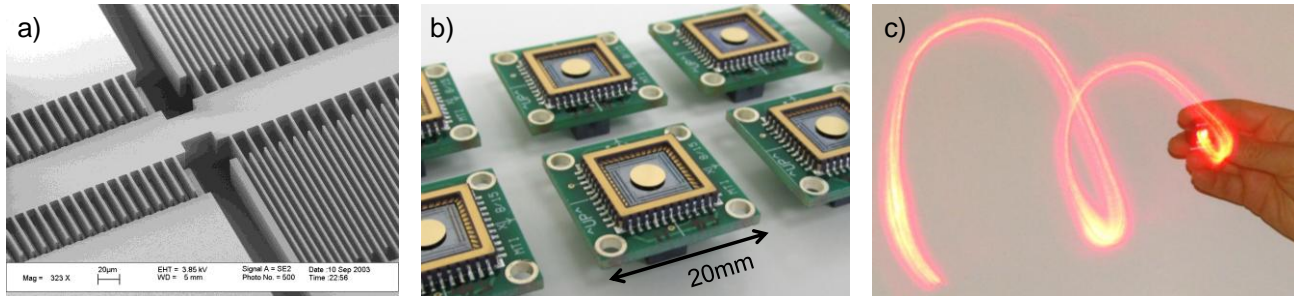


Figure 1 Gimbal-less two-axis MEMS mirrors: a) Multi-level beam vertical combdrive [8] close-up b) MEMS mirrors of 4.2mm diameter in connectorized packages during production [1], c) Tracking application where a MEMS mirror is pointing a laser beam at the small corner-cube reflector held by a person and can track all human movements [6].

## 2.2 Prior work on dielectric-fluid enhanced MEMS

In 2003, McCormick *et al* [9],[10] published a MEMS actuator in which air was replaced as the capacitor dielectric by a dielectric liquid/oil, which resulted in a dramatic increase of capacitance and tuning range while maintaining the small size and modest voltages. Since those publications, there have been surprisingly few publications of immersing MEMS, especially combdrive actuators in dielectric fluids, despite the obvious benefits. Namely, oil capacitors have been used to increase capacitance and reliability of capacitors in extremely high-voltage applications since the days of Nikola Tesla [11]. It has been known to authors through personal discussions and investigation of USPTO applications that multiple companies were experimenting with MEMS mirror enhancement with dielectric fluids [12],[13], and in 2004 Faase *et al* [14] filed a USPTO application describing a “conventional micro-mirror device (which) includes an electro-statically actuated mirror immersed in a dielectric liquid.” The publication essentially states that use of dielectric liquids in arrayed digital MEMS mirrors was a common solution in the art and the inventors refer to the benefits of stiction avoidance but list the fluidic damping as a down-side. Most recently in 2015, Zhang *et al* [15] published a thermally actuated MEMS mirror fully immersed in liquid and demonstrated increased optical scan angle due to the  $>1$  index of refraction of the liquid. In this work the authors are not able to capture the bigger potential benefit like the increase of the dielectric constant because of the different nature of their actuators. Instead, replacing air medium around the thermal actuators with more thermally conductive liquids increases the power consumption of the thermal actuators. Nevertheless, in that work, one of the nice side-benefits of dielectric liquid immersion is clearly demonstrated, i.e. the increased ratio of the optical scan angle to the mirror’s mechanical tilt angle or “optical gain”.

## 2.3 Goal of this Work

In this work, we seek to develop and utilize special packages in which the entire MEMS mirror device is immersed in a dielectric liquid with highly favorable torque-increasing, optical angle-increasing, and damping properties. Replacing air in the rotating electrostatic combdrive actuators with liquids with permittivity higher than air can have a proportional effect of torque increase. Furthermore, by selecting the appropriate fluid viscosity, structural damping could be tuned to a nearly critically-damped point, reducing the overall quality factor of the device from almost 100 to below 1 or a selected number in between. One of the obvious consequences of this favorable damping is a major increase in shock and vibration tolerance. Furthermore, driving of the MEMS mirror can be simplified without the need to cancel unwanted overshoot/ringing by multiple software and hardware methodologies. Namely, the very high quality factors of the silicon MEMS mirrors result in significant driving and controlling challenges. Since these are quasistatic or point-to-point beam steering devices, one of their most natural modes of operation is stepping from one position to another. In Figure 2 we see that the response of a typical gimbal-less MEMS mirror to a step function is an oscillation which can last for 10s of milliseconds or longer. Due to the Q of nearly 100 at the mirror’s resonance, the unfiltered step waveform excites that resonance (2.91kHz in Figure 2 example) – so the beam overshoots to practically twice the desired angle, undershoots back to zero etc. This is clearly highly undesirable and unacceptable in any application, except in special cases where one of the axes is purposely allowed to oscillate at resonance in special raster scanning. Hence, what we must do to avoid such overshoot and ringing is to pre-shape (in time domain) or filter (in frequency domain) the input waveform such that it does not excite the resonant peak which results in a relatively fast step settling time also seen in Figure 2a. But in order to get satisfactory results with a simple low-pass filter (here a 6<sup>th</sup> order Bessel filter is used), we must set the cutoff frequency of the filter to approximately 1/3 of the resonant frequency ( $f_n$ ) of that MEMS mirror. Figure 2b shows this filtered vs. original open loop response and we can see that indeed such a method suppresses the peak adequately but has a severe penalty in available bandwidth. The original -3dB point of the response was at 4500Hz and therefore with some

optimal driving scheme that perfectly inverses the device responses all of that bandwidth would be available. However due to the need to pre-filter which is the simplest but often the only available solution in many applications, the -3dB point drops to 580Hz. It is obvious then that any increased damping and therefore reduction of the Q-factor would allow a much more efficient utilization of the device's full available bandwidth, potentially allowing the use of the full bandwidth without the need for pre-shaping or filtering of command waveforms.

With most dielectric liquids under consideration having a significantly higher thermal conductivity than air, even increased mirror cooling is available for automotive laser lighting applications [16]. Finally, the increased optical scan angle due to the >1 index of refraction of the liquid is an additional benefit.

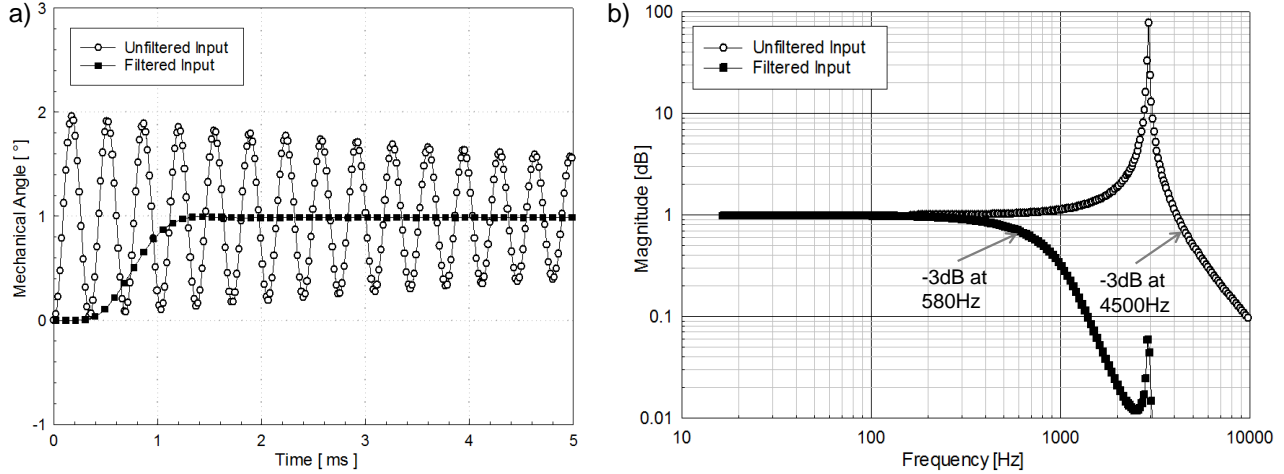


Figure 2. Typical responses of a 1.2mm diameter gimbal-less MEMS mirror in air, showing the challenge of the very high quality factor. (a) step response of the MEMS mirror to unfiltered input vs to input filtered with  $f_c = f_v/3$ , (b) small-signal frequency response of the MEMS mirror with and without the filtered input.

### 3. BASIC THEORY

#### 3.1 Torque Improvement - Permittivity

The rotational motion of electrostatic vertical comb drives is proportional to the torque generated by the electrostatic force of each finger and inversely proportional to the total mechanical stiffness of the rotator and attached structures (mirror etc.) In [17], we show a simple model for calculating the torque of our vertical combdrive structures etched in multi-level approach [8] out of the same monolithic silicon substrate. As seen in (1), torque ( $\tau$ ) is proportional to the square of the voltage ( $V$ ) applied between opposing fingers, and to the derivative of comb finger capacitance ( $C$ ) with respect to angle ( $\theta$ ) which is essentially the tunable capacitance of the combdrive:

$$\tau(\theta) = \frac{1}{2} \frac{dC}{d\theta} V^2 \quad (1)$$

Assuming that the voltage difference is ultimately limited by a variety of factors such as driver design and power consumption, long term reliability, oxide breakdown and comb-finger pull-in, we can maximize this voltage in all designs and cannot obtain any more torque without increasing the tunable capacitance  $dC/d\theta$ . This term is based on the geometry of each finger, number of fingers and of course the permittivity or dielectric constant of the medium between the fingers. Since the comb fingers are rectangular in their cross sections and start with an initial overlap, calculations of exact overlap areas during rotation are more difficult than in the case of traditional lateral comb drives or vertical comb drives in pistoning mode. However, approximations can be made to describe the geometry. The differential area ( $dA$ ) increase can be approximated as a wedge (triangle) from the rotation axis to the rotor fingertip ( $r_2$ ), less the wedge from the rotation axis to the stator fingertip ( $r_1$ ). The desired quantity is calculated from those two triangle areas as follows:

$$\frac{dA}{d\theta} \approx \frac{1}{2} \cdot (r_1^2 - r_2^2) \quad (2)$$

Based on that geometrical factor we can then calculate the tunable capacitance  $dC/d\theta$  as follows:

$$\frac{dC}{d\theta} \approx 2 \frac{\epsilon_0 \cdot \epsilon_r}{g} \cdot \frac{dA}{d\theta} \approx \frac{\epsilon_0 \cdot \epsilon_r}{g} \cdot (r_1^2 - r_2^2) \quad (3)$$

$$\tau(\theta) = N \frac{1}{2} \cdot \frac{dC}{d\theta} \cdot V^2 \approx \frac{N \cdot \epsilon_0 \cdot \epsilon_r \cdot V^2}{2g} \cdot (r_1^2 - r_2^2) \quad (4)$$

Where  $N$  accounts for the number of comb fingers (working together) in the actuator and  $g$  is the gap distance between opposing comb fingers. The factor 2 in (3) comes from the fact that a comb finger has two sides which contribute to the capacitance (it has two opposing fingers). It turns out that the geometrical factors  $r_1$  and  $r_2$  are closely related to angle which the rotator can achieve and should be assumed maximized for a given angle/application – they are also generally limited by chip size. The gap  $g$  is of course a strong factor of manufacturing capabilities and controls; however, it also has a major effect on maximum allowable voltage due to finger lateral stability so it should be assumed that it has already been minimized for a given design. As previously mentioned, if we assume a limited maximum voltage  $V$  and a limited chip size (and thus number of fingers  $N$ ), the only direction of possible torque increase is to replace the air medium with a dielectric fluid. In a dielectric fluid with permittivity higher than air ( $\epsilon_0 \cdot \epsilon_r$ ), the comb drives could obtain proportionally higher torques and therefore a proportional increase in mechanical displacement angle of the mirror.

### 3.2 Quality Factor Reduction - Viscosity

Quality factor in an oscillating resonator is the ratio of the energy stored to the energy dissipated by damping per oscillation cycle, and is (inversely) representative of the damping of the MEMS mirror. For resonators, a high quality factor results in larger displacements, SNR, reduced phase noise, and other benefits. Therefore there is quite a volume of published work on methods to increase quality factor of various types of MEMS resonators, e.g. inertial sensors, reference clock resonators, and resonant mirrors. In many cases such MEMS are used in vacuum to attain extremely high quality factors. But when driving a quasi-static MEMS mirror, the large quality factor results in undesirable overshoots and oscillations as described in Sec. 1.3. In fact, the resonant peak of the quasistatic MEMS mirror is the one part of the response that we typically cannot use. It could be considered ideal to have just that specific portion of the device response cancelled by appropriate driving or control methods such as with closed-loop control or inverse system filtering [19]. Furthermore, a high  $Q$  resonance in a mechanical structure like a MEMS mirror can make it highly susceptible to external environmental perturbation like from shock, vibration, and even sound. This is of concern both in use in terms of positional stability in a perturbing environment and also for overall survivability in major shock/vibe events. If the external perturbation includes frequency content in the vicinity of the high  $Q$  resonance the effect on the structure is magnified, often catastrophically. Despite these multiple obvious benefits of increased damping in the category of MEMS which are to be operated in quasistatic mode, there are practically no publications discussing methods to increase damping.

Here we consider a simple model and propose the benefit of using the viscosity of a dielectric liquid to provide desired damping for the gimbal-less two-axis MEMS mirror. The mirror's mechanical angle is proportional to the angle of driving rotators (rotating vertical combdrive actuators) [17], and the following discussion can be simplified and approximated by considering one complete axis sub-system of the gimbal-less two-axis MEMS mirror as an LTI second order system. This approximation is especially good for integrated (monolithic) MEMS mirrors [20] in which the mirror center of inertia is in the same location as the axis of rotation. Therefore, we proceed with a simplified model with torsional suspensions of the rotator with torsional stiffness  $k$ , and the moment of inertia of the mirror  $I_{MEMS}$ . The model in s-domain can be expressed as:

$$H(s) = G \frac{\omega_n^2}{s^2 + 2\zeta_{air}\omega_n s + \omega_n^2} \quad (5)$$

$$\omega_n = \sqrt{k/I_{MEMS}} \quad (6)$$

where  $G$  is the “voltage-to-angle gain” or mirror rotation per driver voltage,  $I_{MEMS}$  is the moment of inertia of the mirror,  $\zeta_{air}$  is the damping ratio,  $k$  is the torsional stiffness, and  $\omega_n$  is the undamped natural frequency of the system. This 2<sup>nd</sup> order transfer function can very closely match the system plotted in Figure 2b. Furthermore it is interesting to plot a family of curves with increasing damping ratio  $\zeta$ , and to see that the system response becomes more and more like an ideal wideband actuation system with full use of the original -3dB bandwidth.

The damping ratio is proportional to the viscosity of the fluid [21],[22]. Clearly the initial point of the study is viscosity of air which is how the MEMS mirrors are packaged now. Then, the study could look at increasing viscosities and find those which give damping ratio near ideal point of 1.

It should be noted in anticipation of results that the present discussion clearly ignores the likely effect that the density and inertia of the liquid will have on the system response – that is to say that the above transfer function is likely modified in  $\zeta$  as well as in  $\omega_n$  due to a new effective inertia  $I_{MEMS} + I_{FLUID}$ . This will be explored further later.

### 3.3 Optical Gain Improvement – Index of Refraction

In air, or in any uniform light-traveling medium, a single-axis MEMS mirror can steer a beam at an optical angle that is 2 times its mechanical tilt angle (optical gain = 2). As pointed out in [15], Snell's law gives the relationship between incidence angle and refracted angle for light traveling through mediums with different indices of refraction

$$n_1 \sin(\theta)_1 = n_2 \sin(\theta)_2 \quad (7)$$

When considering that a light beam reflecting from a mirror has an angle change that is equal to two times the mechanical angle change of the mirror itself ( $\theta_{\text{mech}}$ ), we can find the optical angle after the beam exits the dielectric fluid medium and re-enters the air with index of 1. For this analysis we assume that the initial optical beam enters the medium (dielectric liquid) normal to the surface and therefore it continues in a straight line to the immersed mirror surface. Then, since the optical angle within the medium is  $2 \cdot \theta_{\text{mech}}$ , upon exit from the medium the final optical angle is:

$$\theta_{\text{opt}} = \sin^{-1}(n_{\text{med}} \cdot \sin(2 \cdot \theta_{\text{mech}})) \quad (8)$$

In practice, we are interested in the optical angle “gain”, meaning the change in  $\theta_{\text{opt}}$  based on the change in mirror tilt  $\theta_{\text{mech}}$ . This gain can be found as the  $d\theta_{\text{opt}}/d\theta_{\text{mech}}$  which has a relatively complex form due to the sin and arcsin functions. It is interesting to quickly analyze small angle approximation to compare the performance with standard in-air performance. Namely, if we assume for small angles that  $\theta \approx \sin(\theta)$ , we can see that:

$$\theta_{\text{opt}} \approx 2 \cdot n_{\text{med}} \cdot \theta_{\text{mech}} \quad (9)$$

Therefore the optical gain is approximately:

$$\frac{d\theta_{\text{opt}}}{d\theta_{\text{mech}}} \approx 2 \cdot n_{\text{med}} \quad (10)$$

Hence, the optical gain is increased from the vacuum/air system value of 2 by the index of refraction of the medium/liquid. This means that additional scan angle factor of over 1.5 is available in such a device for almost any selection of dielectric liquids which is a very significant increase.

We note that for most users of the MEMS mirror based beam-steering technologies, optical resolution ( $\theta^*D$ ) is a key performance figure when comparing technologies and designing systems. This factor shows the ultimate ability of the beam steerer to clearly address separate points in a target field of view with a laser beam. Speed of course is critical as well and very difficult to increase in design, however we must assume that for given reachable speed requirements a designer will seek to find optimal  $\theta^*D$  solution for their optical design. Presently, given certain minimum speed and shock tolerance requirement, the technology is ultimately limited to a  $\theta^*D$  factor somewhere near 35 ( $\pm 7^\circ$  of mechanical angle \* 5mm diameter) unless something different is done technologically, not just by more design iterations. The possibility of multiplying this factor by e.g. 1.5 based on this optical gain or potentially by  $2*1.5$  (torque-increase \* optical gain) is highly motivating for further study. As mentioned earlier there are no other methodologies presently known which could lead to similar increases in the figure of merit for this important technology.

## 4. EXPERIMENTAL SETUP

### 4.1 Selection of Fluids

First, it should be understood that only liquids with favorable optical transmission properties are candidates for such an optical application. After all, the MEMS mirror must have an excellent overall optical reflectance and should not add distortions or astigmatism to the reflected light. This requirement was not imperative for all liquids in our initial tests that focused on the broader search for a good range of viscosities to approximate critical damping, but is critical in future real application of this methodology in products. Liquids such as immersion oils for microscopes were obvious candidates to first experiment with (immersion oil type A - 150cSt and immersion oil type B - 1250cSt). Also, index matching liquids would be great candidates which would match with the fused silica window over the MEMS mirror and thus could actually improve overall transmittance rather than hinder it. In a dielectric fluid (Table 1) with higher relative permittivity, the comb drives could obtain proportionally higher torques and therefore a proportional increase in mechanical displacement angle of the mirror. The fluid should have several other favorable properties in order to be useful in such an application – insulating at high voltages, phase-stable (remain in liquid phase) in a wide range of temperatures, small dependence of viscosity on temperature, etc.

In our initial tests, MEMS devices were packaged and tested with a variety of liquids such as cooking corn oil, automotive oils (brake fluid, hydraulic fluid, engine oil), microscope immersion oils, glycerin, alcohols. Firstly liquids which were not fully insulating at the MEMS actuation voltages were dismissed easily after observing bubbling in the package cavity, e.g. 2-propanol. Also after those initial experiments it became clear that very low viscosities are of

interest, in the range of 0.5cP – 10cP, which reduced the selection quickly and terminated the search for off-the-shelf household items. For example the Type-A immersion oil of 150 cSt resulted in overdamping so significant that we could easily dismiss any liquid with viscosity above e.g. 20 cP for further study. Also in earlier studies we noted the inertia-related reduction of resonance frequency which would result in lower device bandwidth. Therefore further search was focused on low molecular weight and low density liquids with viscosities in the vicinity of 1 cP. Ultimately for the more detailed part of the study we selected two families of dielectric liquids, alkanes and silicon oils and in each case we selected three viscosities (Table 1). The measurements with the package filled with air are the control since the MEMS devices are used in air filled packages in most applications. The second category is Alkanes, specifically Octane, Dodecane and Hexadecane. These liquids have a similar relative permittivity, and vary in kinetic viscosity. The third category consists of silicone oils, which are oils designed to have a specific kinetic viscosity for various applications, and vary in relative permittivity in small increments. One of their important characteristics is that they are designed to have minimal temperature dependence of viscosity. The three silicone oils used are 1cSt, 2cSt oils from Clearco, and a 100cSt oil from Core-RC.

Medium	Relative Permittivity [ $\epsilon$ ]	Kinetic Viscosity [cP]	Density [g/ml]
Air	1	0.019	0.001
<b>Alkanes</b>			
Octane	1.96	0.542	0.703
Dodecane	2.01	1.503	0.750
Hexadecane	2.05	3.474	0.773
<b>Silicone Oil</b>			
Clearco 1cSt	2.29	0.818	0.818
Clearco 2cSt	2.44	1.746	0.873
Core-RC 100cSt	2.73	96.000	0.960

Table 1: A table of all the fluids used for this project. There are two main categories: Alkanes, and Silicone Oils.

#### 4.2 Selection of MEMS Mirrors

Three different MEMS device designs were selected for the study to improve overall performance using various fluids. All three MEMS mirrors are designed for two-axis quasi-static (point-to-point) beam steering with  $\pm 5^\circ$  mechanical tip/tilt angle and based on a gimbal-less, monolithic structure with vertical comb drive actuator design. The three MEMS devices are Aluminum coated, vary in mirror diameter and consequently the device bandwidth and resonant frequency. The selected designs are:

MEMS Device Design	Mirror Diameter [ $\mu\text{m}$ ]	Chip Die Size [mm x mm]	Mechanical Angle* [ $^\circ$ ]	Resonant Frequency* [Hz]
A3I8.2	800	4.25 x 4.25	+/-6 $^\circ$	3900
A3I12.1	1200	4.25 x 4.25	+/-5 $^\circ$	2700
A7M20.1	2000	5.20 x 5.20	+/-5 $^\circ$	1300

Table 2: A table of the three MEMS device designs used in this project. \*Note: The mechanical angle and resonant frequency defined in the table are in standard, air-filled packages.

#### 4.3 Characterization Methodology

The characterization of the MEMS devices for this study is performed on two stations. The first is a 20mm x 20mm Position Sensitive Detector (PSD) (Figure 3a) used to measure the MEMS device's tip/tilt angle, frequency response and step response by reflecting a laser beam off the MEMS mirror onto the PSD's face. The MEMS device is driven by a BDQ Amplifier [20], connected to a PCI-based NI-DAQmx card. The NI-DAQmx card drives the MEMS device, observes the drive voltages, and the resulting scan from the PSD. The driver voltages and the PSD measurements are used to calculate and plot the various parameters used to describe the MEMS device such as voltage vs. angle gain, frequency response, step response, resonant frequency, quality factor, etc. Typically, the MEMS device is facing the PSD normally, approximately 30mm away, with a  $\sim 20^\circ$  angle of incidence from the CW laser. This allows the PSD to characterize the MEMS device, and produce a datasheet with the device's parameters. For this study, the test setup is modified to have the MEMS device in a DIP24 package, mounted on a PCB with a ZIF socket for easy insertion/removal, placed flat on the test bench table facing up. The PSD is placed at a glancing angle to the MEMS device and a laser beam at  $\sim 25^\circ$  angle of incidence to the MEMS mirror is reflected onto the PSD. Multiple

measurements are run as the package cavity with the MEMS device is filled with different fluids (Figure 3d). This station is used to measure the change in damping ratio with the frequency response and step response measurements, and the final optical angle gain with the voltage vs. angle plots. The voltage vs. angle plots are limited to small angles since the PSD is limited in size, and is located at a distance where angles larger than 2° fall outside of the PSD's measurement surface.

The second test setup is a Bruker Contour-GT-K Optical Microscope (Figure 3b), typically used to measure surface flatness of the MEMS mirrors. For this project, the microscope is used to measure the mechanical tilt angle of the MEMS mirror when the same voltage is applied but the package cavity with the MEMS device is filled with different fluids. To achieve these measurements, the MEMS device is placed in a PCB with a ZIF socket for easy insertion/removal and the PCB is placed on a 5 degree-of-freedom stage for proper accurate alignment (Figure 3c) for the microscope's measurement. A USB-SL MEMS controller is used to drive the MEMS device to a tilted position when the microscope is ready to take a measurement.

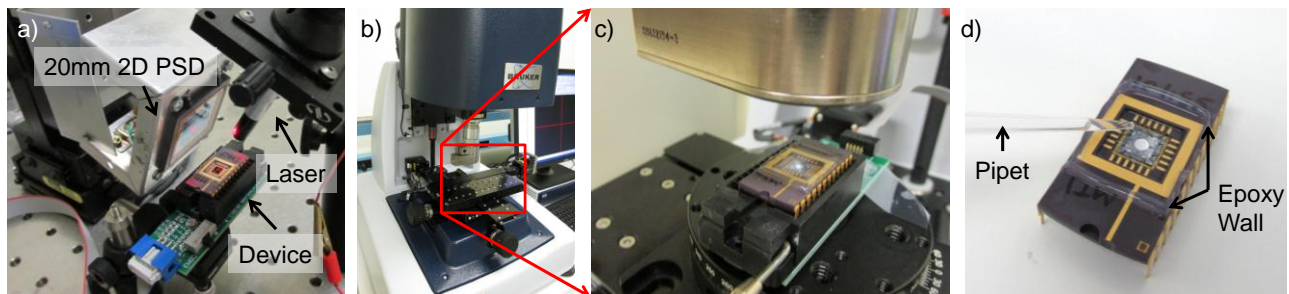


Figure 3 Experimental Setup – (a) Frequency and Step Response measurement of a device on the PSD Test Setup, (b) Bruker Contour-GT-K Optical Microscope used for MEMS mirror mechanical tilt measurements, (c) Close up of the MEMS device under measurement on the optical microscope, (d) MEMS package being filled with fluid using a pipette.

#### 4.4 Packaging Methodology

Possible methodologies for reliable packaging of the MEMS mirrors with selected dielectric liquids was considered from the start of the project for two reasons. Firstly, it is important to consider real-world implications of the work in terms of the real possibility of series production of such enhanced MEMS mirror devices. Producing some highly promising results without a clear path to their possible real-world application and availability would be futile although still quite interesting academically. The second reason was very practical - it was easier to perform initial experiments with several already packaged devices by adding a liquid under test and sealing them with a window and epoxy. In such a closed form we could mount the device in our standard side-facing test stations (Figure 4c) and use them in the laboratory more freely. Therefore even the very first experiments to see any effects of various oils and other liquids were accruing experience in the challenges and solutions for reliable packaging. Ultimately, this topic is very much a work in progress but here we outline some findings to date.

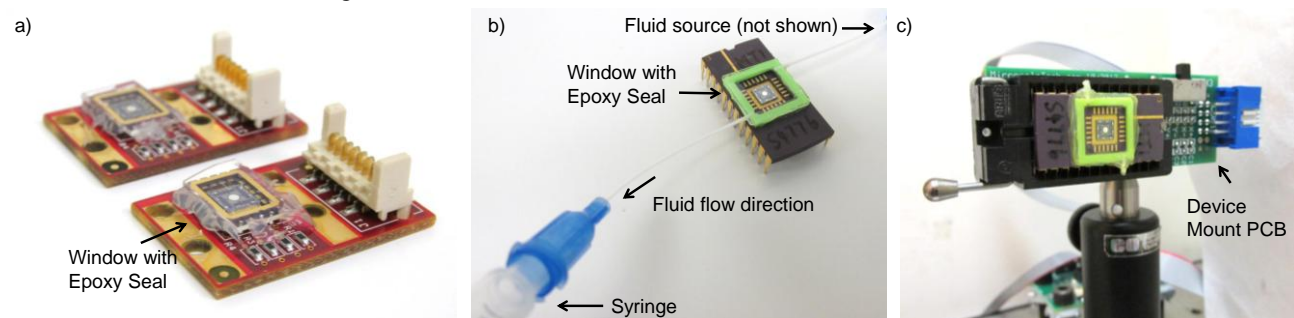


Figure 4 Packaging methodologies for prototyping a) early version with epoxy sealed window to contain the liquid, b) Filling up the MEMS device with liquid while removing air from the package, c) Complete prototype packaging

Figure 4a shows the earliest packaging experiments. Here some non-compliant devices from a serial production process were taken for R&D purposes. Each was given a different liquid by pipette until the liquid reached over the top edge but did not spill. Then, an AR-coated (in this case not properly matching the liquid but one side correctly matching air) window was slid over the top in attempts to minimize bubble formation and trapping under the window. Having

excessive liquid resulted in lower chances of a trapped bubble although leaving the overall connectorized TinyPCB package more messy. Then, the window was pressed down by a tool while UV-curable epoxy was applied around the outside edges between the window which overhangs the carrier and the board below. Pressure was kept on the window during curing. Thus the window was kept in place. This sealing method was found adequate for months of experimentation with the same unit in terms of minimal evaporation and no leaking of the liquid, although quite messy and not capable of fully preventing bubble formation. Besides the obvious bubbles trapped at the interface with the glass cover, air trapped in the combdrive or below the mirror in the device was found to be the key challenge in packaging.

The next design shown in Figure 4b and Figure 4c incorporated a pre-sealed package with only two small diameter feeding tubes accessing the package cavity. One of the tubes was inserted in the liquid and the other was attached to a syringe which provided enough vacuum to remove the air in the package and pull in the liquid. Here we obtained much better results in reducing trapped air. After the process the tubes are cut and sealed off with epoxy – the process was found to be relatively simple.

As mentioned above the topic of packaging is work in progress but it has been found so far that the problem is not expected to be insurmountable. Moreover it is known that solutions for fluidic packaging of MEMS in e.g. inkjet printer heads have been well established in industry for decades and therefore mass-production is also expected to be very doable and low cost.

## 5. RESULTS

### 5.1 Torque Improvement – Permittivity

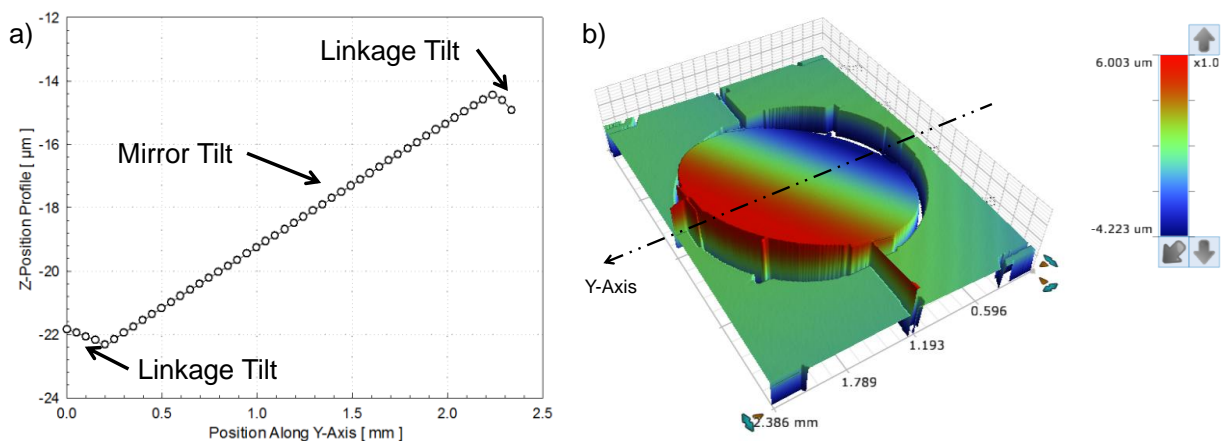


Figure 5. Example of measurement of mirror and actuator mechanical angle with the 3D optical microscope. a) Measured Mirror surface height profile along the x-axis of rotation b) 3-D contour figure showing the tilt of the MEMS mirror

A Bruker 3D optical microscope was used to determine the mechanical tilt of the MEMS mirror and its rotators. Compared to measuring the tilt angle on a PSD, the measurement in this process was not dependent on the index of refraction since it directly measures the mechanical 3D shape of the MEMS mirror structure. In each test, for a given MEMS mirror or given liquid or actuation voltage being tested, a VSI (vertical scanning interferometry) measurement was taken which produced a 3-D profile (Figure 5b). Then, surface heights along the cross-section orthogonal to the axis of rotation were extracted and plotted as shown in the example of Figure 5a. In that example we can clearly measure both the angles of the rotator linkages leading up to the mirror as well as the angle of the mirror itself. In general this procedure was very difficult with dielectric liquid samples due to a variety of reasons. One of the reasons was that the surface curvature of the liquid “bath” in the package cavity made measurements distorted and difficult. Another was that evaporation, albeit slow, would continually move the apparent location of the device in the microscope etc. Adding the alkanes to the MEMS package cavity interfered with the measurement and did not produce any valid data due to a lack of contrast, especially when the mirror was tilted. Therefore the only reliable results were obtained with silicon oils, as shown in Figure 5 and Table 3. Overall, the addition of dielectric fluid and resulting increase of permittivity led to a substantial increase in the rotator torque and mechanical mirror angle. The increases in all cases are close to the expected factor of  $\epsilon_r$  but in each case are approx. 20% higher than expected. Because of the difficulty of these experiments we

were not able to conclusively state whether the torque and angle increases are indeed above the expected or whether the data has errors and further study is necessary.

A3I12 Device in Medium	Relative Permittivity [ $\epsilon$ ]	Mechanical Angle Per Volt [ $^{\circ}/V$ ]
Air	1.00	0.0354
Clearco 1cSt	2.29	0.0968
Clearco 2cSt	2.44	0.1070
Core-RC 100cSt	2.73	0.1142

Table 3: List of liquids used in the experiments – shown with their relative permittivity, and mechanical tilt.

### 5.2 Reduction of Quality Factor – Viscosity

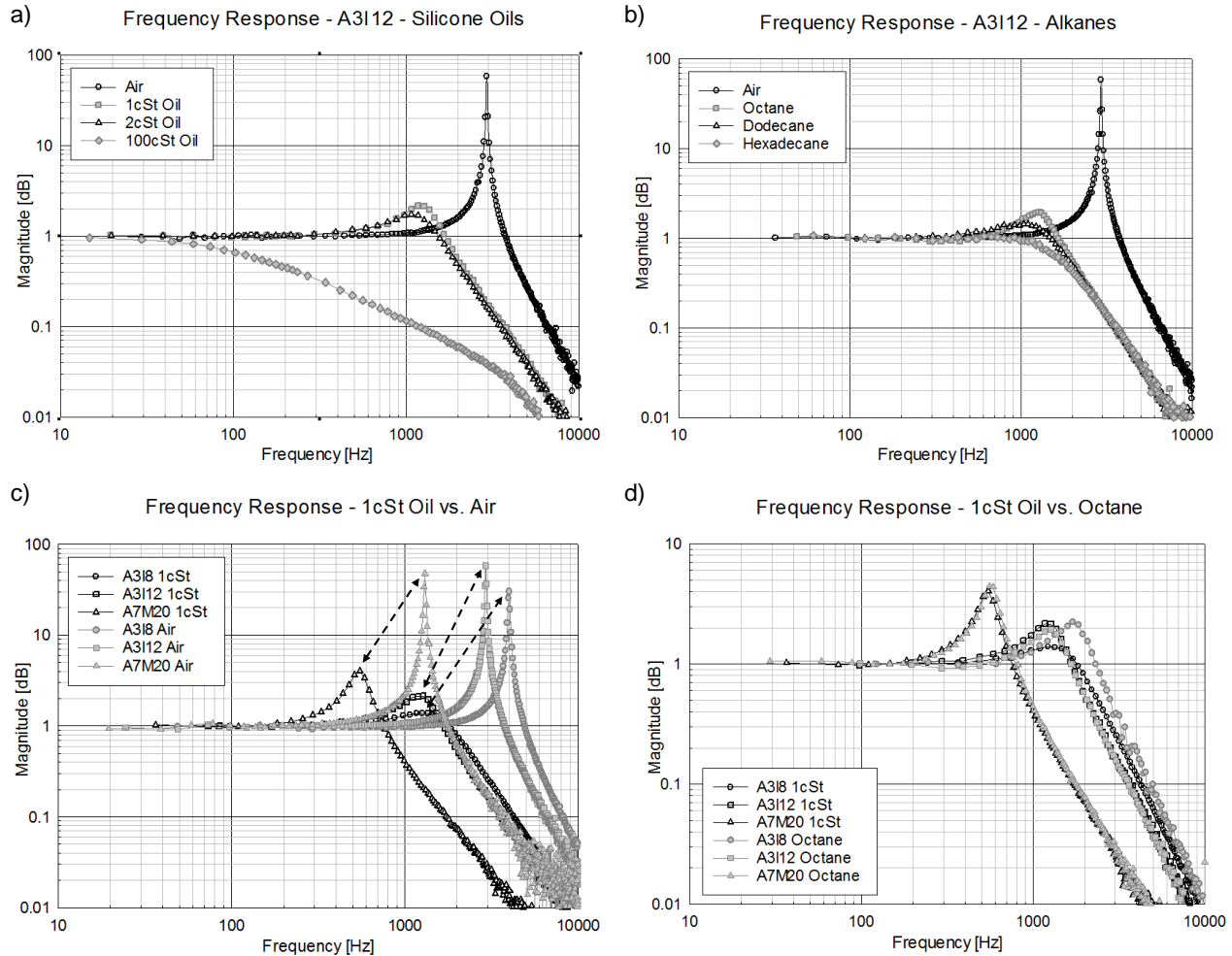


Figure 6. Measured frequency responses of various samples in air and different dielectric liquids (normalized magnitudes plotted): a) One mirror (1.2mm) in air and 3 viscosities of oils (1cP, 2cP, 10cP), b) One mirror (1.2mm) in air and 3 viscosities of alkanes (Octane, Dodecane, Hexadecane), c) Three mirror sizes in air and in Clearco 1cSt Oil, d) Three mirror sizes, 1cSt Oil vs Octane

As seen in the Figure 6, the viscosity of the fluids has a major effect on the quality factor of the MEMS mirrors. What can also be seen in the figure is that there is significant effect on the resonant frequency of the device as well, shifting all the response curves down and to the left. Figure 6a and Figure 6b show the A3I12 MEMS mirror frequency response in silicone oils and alkanes respectively. Here we specifically targeted a few increasing viscosities to see a family of curves and trends. The tallest peak (Air) on the right of both graphs shifts lower in frequency and decreases in magnitude as the viscosity of the dielectric fluids increases. The initial shift of frequency to the left seems to be due to density/inertia

property of the liquid and not really viscosity dependent. Further shift to the left between the difference curves should be attributed to the fact that the damped resonance continues to decrease from its undamped value with increasing damping ratio.

The results show that the amount of damping is completely adjustable by simply choosing a dielectric fluid with a desired viscosity to reach the damping specification. Figure 6c shows the effect of a particular dielectric fluid on different mirror sizes. Here we have measurements of three mirror sizes in air and the same mirrors in 1cSt Oil. The left and down shift of the resonant peak is clearly seen for each case. The smaller mirror (A318 - 0.8mm diameter) had the largest increase in damping while the largest mirror (A7M20 - 2mm diameter) had the smallest increase in damping. In terms of the reduction of resonant frequencies by the apparent addition of a new inertia ( $I_{FLUID}$ ), the effects appear to be the same in the three mirror sizes and this effect requires further study. One deeper look into the effect is shown in Figure 6d compares two different fluids with similar viscosity but somewhat different densities. It would have been interesting to experiment with liquids of very different densities but the values of available media were relatively close. Although this data is preliminary and effect small because of similar densities, the data does show the correct trend – that the curves have additional left-shift in silicone oils which have a higher density.

**5.3 Optical Scan Angle Improvement – Index of Refraction**

Measurements of optical scan angles on the PSD showed increase in final optical scan angle due to the combined effect of increased torque (from liquid’s relative permittivity) and the optical gain (from liquid’s index of refraction). Since the maximum achievable scan angles were much larger than could be fit onto the PSD in the given setup shown in Figure 3a, we performed measurements with reduced voltages chosen to ensure that they would fit in the PSD area. Specifically we were only interested in testing the slope of drive voltage vs. scan angle near the origin to compare air and liquid-filled packages. The slopes were extracted near origin from ramp response measurements from -15V difference to +15V difference (Figure 7b). It is immediately evident in the ramp responses that the highest angle gain is present in the case of the dielectric liquid with the highest permittivity. Note that in Figure 7b some measurements such as Air, Octane and the 2cSt Silicone Oil provided a linear measurement, however the 100cSt measurement started showing non-linearity at Vdifference > 10V which was not understood.

From our simple models in Sec. 2 we anticipated that the optical scan angle would be increased both by the permittivity and by the index of refraction which can be approximated as the square root of permittivity for the materials where it is not specifically available. Therefore we anticipated relationships of  $\epsilon_r * \epsilon_r^{1/2}$  among the measured samples. This is matched quite well by the measured slopes as clearly seen in the table in Figure 7a. For that data, the same device’s optical angle was measured with different fluids at the same voltage difference. The calculated value in the fourth column is based on the air-filled package value multiplied by  $\epsilon_r^{3/2}$ .

a)

A3112 Device in Medium	Relative Permittivity ( $\epsilon_r$ )	Measured Optical Angle / Volt [ $^{\circ}/V$ ]	Calculated Optical Angle / Volt ( Air Value * $\epsilon_r * \sqrt{\epsilon_r}$ ) [ $^{\circ}/V$ ]
Air	1	0.0198	0.0198
Octane	1.96	0.0555	0.0543
Dodecane	2.01	0.0561	0.0564
Clearco 2cSt	2.44	0.0750	0.0755
Core RC 100cSt	2.73	0.0844	0.0893

b)

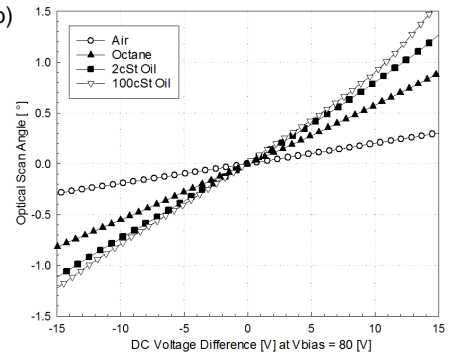


Figure 7. a) A table of optical angle measurements of A3112 device packaged with different fluids with permittivities as listed. Measured vs. Calculated Optical Angle / Volt values are given. b) Plots of ramp responses of the A3112 device in a few mediums showing increased slopes approximately proportional to  $\epsilon_r * \epsilon_r^{1/2}$ .

**6. CONCLUSIONS**

The numerous anticipated benefits of packaging gimbal-less two-axis MEMS mirrors with dielectric liquids were clearly experimentally demonstrated. Use of the dielectric liquids enabled doubling and in some cases tripling of the previously achieved  $\theta * D$  product while still maintaining speeds applicable for many tracking, LiDAR, and related applications. This has been demonstrated with varied actuators and mirror sizes. To re-demonstrate the magnitude of the findings more visually, we look at the beam scanning results in Figure 8 where we point a laser beam at the mirror scanning 20Hz

circles on a calibrated wall. The device is driven modestly at about 40% of its usual range and in Figure 8a it achieves  $\pm 5.2^\circ$ . In Figure 8b, in hexadecane-filled package the optical angle is increased to  $\pm 14.7^\circ$ . We note in Figure 8b that the scan is showing saturation effects because the combdrives are reaching full stroke. Since all of the MEMS mirrors tested in this study were specifically designed and optimized for operation in air, the full potential of the dielectric liquid packaging could not yet be demonstrated. Namely, in a new design where the increased permittivity and optical gain are given at the start of the design, the parameter space can be traded differently and optimized quite a bit further in the direction most useful to the application.

It was also found that packaging adequately with chosen dielectric liquids will require more development but is likely to be a problem that can be successfully and inexpensively solved. At the time of this publication, some of our samples sealed with silicone oils 13 months ago using the ad-hoc epoxy-sealed packaging method (Figure 4a) continue to operate. The increased  $\theta \cdot D$  product figure of merit seemingly comes at the expense of reduced resonant frequency due to the density of the liquid presenting additional inertia in the system. This was observed as the left-shift of all of the frequency response plots and is the only notable downside to the utilization of the liquids found so far. However when comparing to above-mentioned presently used open-loop (feed forward) methods to avoid overshoot and ringing, the loss of bandwidth is not significant or not present at all. Overall, with results to date, similar or same useable bandwidth is achieved while the angle is greatly increased.

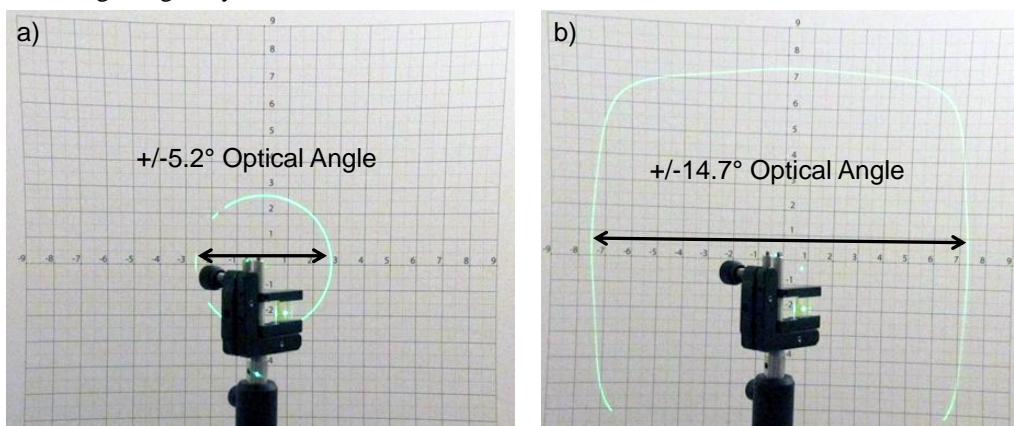


Figure 8. Example of A3112 MEMS mirror scanning a beam on a calibrated wall with  $V_{\text{difference}}=50\text{V}$  and  $V_{\text{bias}}=80\text{V}$ : (a) in air-filled package scanning reaching  $\pm 5.2^\circ$  optical and (b) in hexadecane-filled package reaching  $\pm 14.7^\circ$  optical.

The increased figure of merit does not change the compactness and low power-consumption of the MEMS-based beam-steering solution since the improved MEMS mirrors still consume  $<1\text{mW}$  in operation and drivers typically consume  $100\text{mW}$ . The MEMS mirror PCB and its digital-input driver PCB are approximately  $25\text{mm} \times 25\text{mm} \times 15\text{mm}$  in volume and weigh only  $<15\text{g}$ .

One of the most exciting benefits of the packaging methodologies is that the damping dramatically increases shock and vibration tolerance. This has so far been tested only informally by dropping various exposed device packages from different heights  $>1\text{m}$  onto the metal optical bench surface. In these informal tests the liquid-packaged MEMS have survived 100% of the time while air-packaged MEMS often broke.

## 7. REFERENCES

- [1] Mirrorcle Technologies, Inc. Website, Support Page 2016, <http://mirrorcletech.com/support.html>, March, 2016.
- [2] Keshavmurthy, S.P., *et al*, "Non-contact Sensing System Having MEMS-based Light Source," Patent No. US20120062706 A1, March 15, 2012.
- [3] Chen D. Lu, Martin F. Kraus, Benjamin Potsaid, Jonathan J. Liu, WooJhon Choi, Vijaysekhar Jayaraman, Alex E. Cable, Joachim Hornegger, Jay S. Duker, and James G. Fujimoto, "Handheld ultrahigh speed swept source optical coherence tomography instrument using a MEMS scanning mirror," Biomed. Opt. Express 5, 293-311 (2014)
- [4] Moss, R., Yuan, P., Quesada, E., Sudharsanan, R., Stann, B., Dammann, J., Giza, M., Lawler, W., "Low-cost compact MEMS scanning lidar system for robotic applications", Proc. SPIE 8379, Laser Radar Technology and Applications XVII, 837903, May, 2012

- [5] Spectrolab Website, SpectroScan 3D MEMS LIDAR System Model MLS 201 Datasheet, 2012, [http://www.spectrolab.com/sensors/pdfs/products/SPECTROSCAN3D\\_RevA%20071912.pdf](http://www.spectrolab.com/sensors/pdfs/products/SPECTROSCAN3D_RevA%20071912.pdf), March 2016.
- [6] Milanović, V., Siu, N., Kasturi, A., Radojičić, M., Su, Y., ""MEMSEye" for Optical 3D Position and Orientation Measurement," Proc. SPIE 7930, MOEMS and Miniaturized Systems X, 7930-27, March, 2011.
- [7] Richter, S., Stutz, M., Gratzke, A., Schleitzer, Y., Krampert, G., Hoeller, F., Wolf, U., Doering, D., "Position sensing and tracking with quasistatic MEMS mirrors," Proc. SPIE 8616, MOEMS and Miniaturized Systems XII, 86160D, March, 2013.
- [8] Milanović, V., "Multilevel-Beam SOI-MEMS Fabrication and Applications," IEEE/ASME Journal of Microelectromechanical Systems, vol. 13, no. 1, pp. 19-30, Feb. 2004.
- [9] D. T. McCormick, Z. Li and N. C. Tien, "Silicon MEMS Tunable Capacitors Operating in Dielectric Fluid" Proc. TRANSDUCERS '03, Solid-State Sensors, Actuators and Microsystems, 12th International Conference on, Vol.1, p. 871-874, June 2003.
- [10] D. T. McCormick, Z. Li and N. C. Tien, "Dielectric Fluid Immersed MEMS Tunable Capacitors" Proc. Microwave Symposium Digest, 2003 IEEE MTT-S International, Vol. 1, p. 495-498, 8-13 June 2003.
- [11] Tesla, N., "Electrical Condenser," Patent No. US464667 A, Dec, 8, 1891
- [12] Last, M., CrossFiber Inc., in discussion with author, 2011.
- [13] McCormick, D. T., Advanced MEMS Inc., in discussions with author, 2007-2011.
- [14] Faase, K., Jilani, A., Guo, J., Cruz-Uribe, T., "Micro mirror device with adjacently suspended spring and method for the same," Patent No. US6999228 B2, Feb, 14, 2006.
- [15] Zhang, X., Zhang, R., Koppal, S., Butler, L., Cheng, X., Xie, H., "MEMS mirrors submerged in liquid for wideangle scanning," in "Solid-State Sensors, Actuators and Microsystems (TRANSDUCERS), 2015 Transducers-2015 18th International Conference on," (IEEE, 2015), pp. 847–850.
- [16] Kasturi, A., Milanović, V., Yang, J., "MEMS Mirror Based Dynamic Solid State Lighting Module," Journal of the Society for Information Display, Display Week 2016, May 2016.
- [17] Milanović, V., Matus, G., McCormick, D.T., "Gimbal-less Monolithic Silicon Actuators For Tip-Tilt-Piston Micromirror Applications," IEEE J. of Select Topics in Quantum Electronics, vol. 10, no. 3, pp. 462-471, Jun. (2004).
- [18] Milanović, V. "Linearized Gimbal-less Two-Axis MEMS Mirrors," 2009 Optical Fiber Communication Conference and Exposition (OFC'09), San Diego, CA, Mar. 25, 2009.
- [19] Milanović, V., Castelino, K., "Sub-100  $\mu$ s Settling Time and Low Voltage Operation for Gimbal-less Two-Axis Scanners," IEEE/LEOS Optical MEMS 2004, Takamatsu, Japan, Aug. 2004
- [20] Mirrorcle Technologies, Inc. Support Page, "Mirrorcle Technologies MEMS Mirrors – Technical Overview," <http://mirrorcletech.com/pdf/Mirrorcle%20Technologies%20MEMS%20Mirrors%20-%20Technical%20Overview.pdf>, March 2016
- [21] Sandner T., Klose, T., Wolter, A., Schenk, H., Lakner, H., Davis, W., "Damping analysis and measurement for a comb-drive scanning mirror", Proc. SPIE 5455, MEMS, MOEMS, and Micromachining, 147, August, 2004
- [22] Berny, A., "Substrate Effects in Squeeze Film Damping of Lateral Parallel-Plate Sensing MEMS," in <http://www-bsac.eecs.berkeley.edu/~pister/245/project/Berny.pdf>.